Lake surface water temperature [in "State of the Climate in 2019"]

Carrea, L., Woolway, I., Merchant, C., Dokulil, M. T., De Gasperi, C. L., de Eyto, E., Kelly, S., La Fuente, R. S., Marszelewski, W., May, L., Paterson, A. M., Pulkkanen, M., Rusak, J. A., Rusanovskaya, O., Schladow, S. G., Schmid, M., Shimaraeva, S. V., Silow, E. A., Timofeyev, M. A., Verburg, P., Watanabe, S. and Weyhenmeyer, G. A. (2020) Lake surface water temperature [in "State of the Climate in 2019"]. Bulletin of the American Meteorological Society, 101 (8). S26-S28. ISSN 1520-0477 doi: https://doi.org/10.1175/2020BAMSStateoftheClimate.1

Table 2.1. Temperature anomalies (°C) and uncertainties (where available) for 2019 w.r.t. the 1981–2010 base period. Where uncertainty ranges are provided, the temperature anomalies correspond to the central values of a range of possible estimates. Uncertainty ranges represent a 95% confidence interval. Note that for the HadCRUT4 column, land values were computed using the CRUTEM.4.6.0.0 dataset (Jones et al. 2012), ocean values were computed using the HadSST.3.1.1.0 dataset (Kennedy et al. 2011a,b), and global land and ocean values used the HadCRUT4.6.0.0 dataset (Morice et al. 2012).

Global	NASA-GISS (°C)	HadCRUT4 (°C)	NOAA GlobalTemp (°C)	ERA5 (°C)	JRA-55 (°C)
Land	+0.83	+0.70 ± 0.13	+0.78 ± 0.14	+0.87	+0.78
Ocean	+0.38	+0.38 ± 0.07	+0.40 ± 0.16	+0.48	+0.39
Land and Ocean	+0.56 ±0.05	+0.44 ± 0.08	+0.51± 0.15	+0.59	+0.51

For 2019, the reanalyses also show warmer-than-average conditions over many regions of the world (Figs. A2.3, A2.4), particularly over high northern latitudes. Over both global ocean and global land, the two reanalyses agree that the 2019 2-m air temperature was the second highest on record and that the last five years (2015–19) were the five warmest years on record over both global ocean and global land (as well as globally).

2) Lake surface temperature—L. Carrea, R. I. Woolway, C. J. Merchant, M. T. Dokulil, C. L. DeGasperi, E. de Eyto, S. Kelly, R.S. La Fuente, W. Marszelewski, L. May, A. M. Paterson, M. Pulkkanen, J. A. Rusak, O. Rusanovskaya, S. G. Schladow, M. Schmid, S. V. Shimaraeva, E. A. Silow, M. A. Timofeyev, P. Verburg, S. Watanabe, and G. A. Weyhenmeyer

In 2019, the worldwide averaged satellite-derived lake surface water temperature (LSWT) warm-season (June–August in the Northern Hemisphere [NH]; December–February 2018/19 in the Southern Hemisphere [SH]; and December–August 2018/19 for the tropical region of 23.5°N–23.5°S) anomaly was +0.025 ± 0.022°C compared with the 1996–2016 base period. The mean warming trend from 1995 to 2019 was 0.21 ± 0.02°C decade^{-1}, broadly consistent with previous analyses (Woolway et al. 2017, 2018; Carrea et al. 2019). On average, anomalies (with respect to the 1996–2016 baseline) in 2019 were less positive than in 2018 and in 2017, *0.*23°C and 0.19°C less, respectively. The warm-season anomalies for each lake are shown in Plate 2.1b. Per lake, the LSWT anomaly was positive for 47% of lakes, and negative for 53%. Some similarities between the 2019 warm-season lake temperature anomalies and the ice cover anomalies, in terms of spatial distribution in the NH (Sidebar 2.1; Fig. SB2.1), can be observed in regions where longer ice duration is related to negative lake water temperature anomalies.

In the NH, distinctive warmer and cooler regions can be identified: Alaska, Greenland, Europe (except the northeast) show clearly positive anomalies, while Tibet and parts of North America show clear

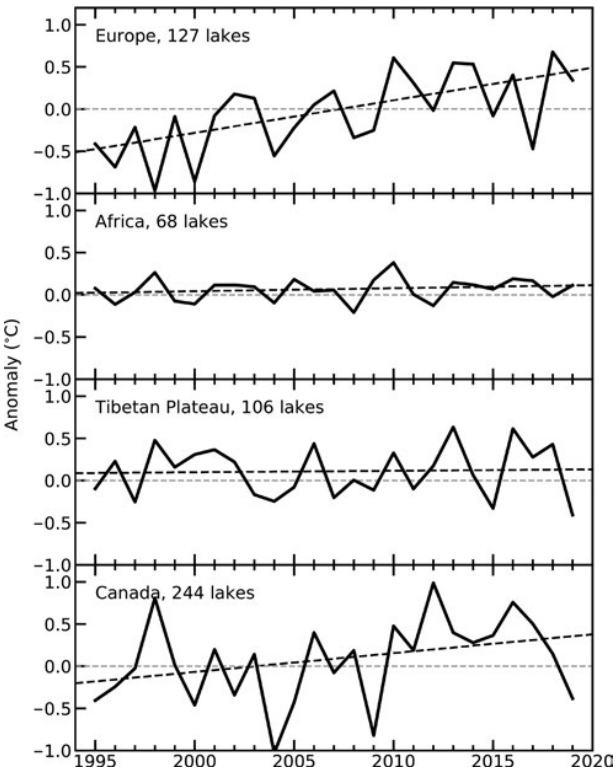

Fig. 2.2. Satellite-derived annual LSWT anomalies (°C; relative to 1996–2015) from 1995 to 2019 for Europe, Africa, Tibet, and Canada. These values were calculated for the meteorological warm season (Jun–Aug in the NH; Dec–Feb in the SH; and over the whole year in the tropics).

negative anomalies. Four regions are shown in more detail: Europe (n = 127), Tibet (n = 106), Africa (n = 68), and Canada (n = 244). The warm-season LSWT calculated from the satellite data shows a warming tendency of +0.39 ± 0.03°C decade^{-1} in Europe and +0.22 ± 0.04°C decade^{-1} in Canada. In Africa and Tibet the tendency is more neutral (Fig. 2.2.). The year 2018 was the warmest since records began in 1995 for European lakes over the June–August (JJA) period (similar to the finding for July–September [JAS] in Carrea et al. 2019). The anomaly in Europe in 2019 was more moderately positive than in 2018, due to the contribution of cooler lakes in northern Europe and Ireland (see section 7f for details). In particular, the border between Scandinavia and Finland delimits regions with contrasting behaviors, i.e., positive anomalies for Scandinavia and a few negative anomalies for Finland and the Karelia region of Russia, respectively. Modeled lake temperature anomalies in the ECMWF ERA5 reanalysis (Hersbach et al. 2020) are available that include lakes smaller than are observable in the satellite data (≥ ~1 km^2), modeled as the fraction of each land surface grid cell covered by inland water (so-called "lake tiles"). The reanalysis lake tile temperatures are shown in Fig. 2.3. For the lakes in Ireland, the observed LSWT anomalies are moderately negative in contrast to the moderately positive ERA5 modeled data, while LSWT anomalies from satellite data are generally consistent with the ERA5 data in Canada, Tibet, and Africa (Fig. 2.3). ERA5 data are driven by the reanalysis surface meteorological conditions (Balsamo et al. 2012) and in general, the lake temperature anomalies broadly track observed air temperature, although factors such as wind speed, humidity, insolation, and the thermal time constants of lakes influence variations within this broad pattern.

LSWT time series were derived from satellite observations from the series of Along Track Scanning Radiometers (ATSR) and the Advanced Very High Resolution Radiometers (AVHRR) on MetOp A and B platforms. The retrieval method of MacCallum and Merchant (2012) was applied on image pixels filled with water according to both the inland water dataset of Carrea et al. (2015) and a reflectance-based water detection scheme. The satellite-derived LSWT data are spatial averages for each of a total of 927 lakes, for which high-quality temperature records were available through August 2019. Lake-wide average surface temperatures have been shown to give a more representative picture of LSWT responses to climate change than single-point measurements (Woolway and Merchant 2018). In addition, in situ LSWT observations have been analyzed (n = 32) for which long time-series are available.

Eighty-one percent (n = 26) of lakes with in situ LSWT measurements were found to have positive anomalies in

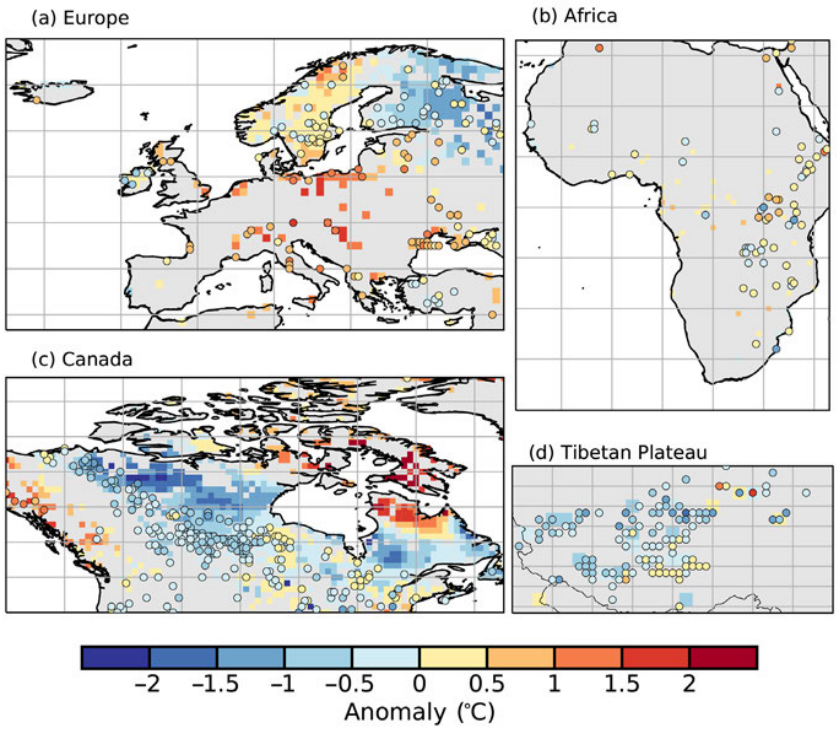

Fig. 2.3. Satellite-derived LSWT anomalies in 2019 (colored points) together with surface lake water temperature from the ECMWF ERA5 modeled data in Europe, Africa, Canada, and Tibet. The two sets of LSWT anomalies (°C; relative to 1996–2015) are calculated for the meteorological warm season (Jun–Aug in NH; Dec–Feb in SH; and over the whole year in the tropics).

2019. Similar to the satellite data, positive anomalies were found for Europe in 2019. For example, the second-largest lake in Sweden by surface area, Vättern, experienced an LSWT anomaly of +0.98°C in 2019, while that of Mondsee, Austria, was +2.1°C. The average LSWT anomaly in lakes with in situ data was +0.6 ± 0.15 °C in 2019, which is substantially higher than the global average anomaly calculated from the satellite-derived observations (+0.025°C). This difference can be due to various factors, including the restricted global coverage of lakes with in situ data (these lakes are primarily situated in Europe and North America), the difference in lake size among the datasets (more lakes with in situ data tend to be small) and, unlike the in situ observations, which are restricted to a single point within a lake, the satellite data capture the intra-lake heterogeneity of LSWT anomalies, thus capturing within-lake regions that are either warming rapidly or experiencing relatively minimal change (Woolway and Merchant 2018).

3) Land and marine temperature extremes—R. J. H. Dunn, S. Perkins-Kirkpatrick, R. W. Schlegel, and M. G. Donat

Over land, 2019 recorded the most number of warm days (TX90p, see Table 2.2 for definition) in the record dating to 1950, with over 60 days compared to the average of 36.5 (Fig. 2.4). The number of cool nights (TN10p) was low compared the last 70 years, but above average for the most recent decade. As the spatial coverage of the in situ GHCNDEX (Donat et al. 2013) dataset is not complete due to delayed or lacking report of up-to-date station data in many regions, the time series from the ERA5 reanalysis (Hersbach et al. 2020; Fig. 2.5; Fig. A2.5) is also shown. A similar picture emerges, but the number of warm days does not exceed the record maximum set in 2016. Similarly, the number of cool nights is also close behind the record minimum of 2016. Differences with GHCNDEX may be the result of the more complete coverage of ERA5.

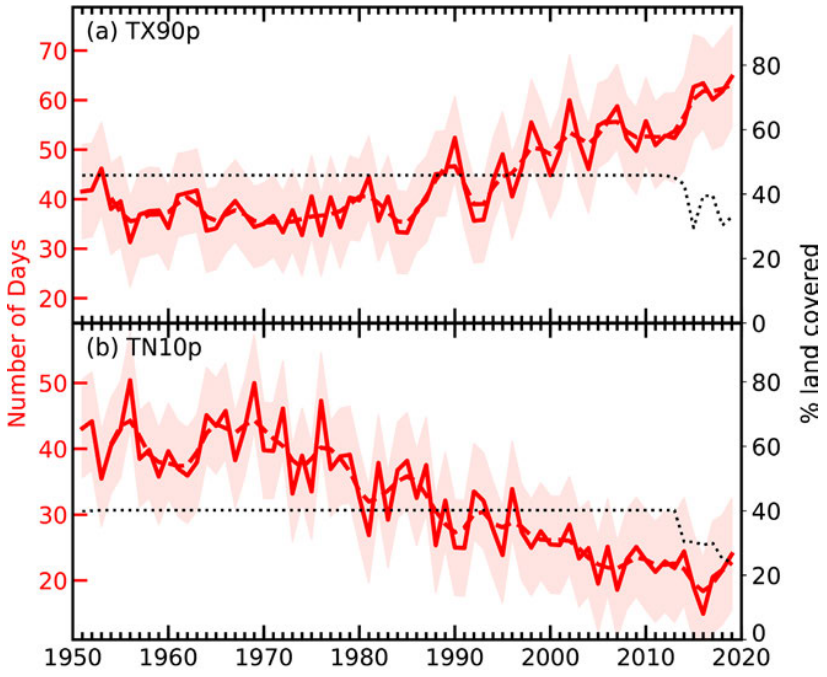

Fig. 2.4. Time series of (a) TX90p (warm days) and (b) TN10p (cool nights). The red dashed line shows a binomial smoothed variation, and the shaded band the uncertainties arising because of incomplete spatio-temporal coverage estimated using ERA5 following Brohan et al. (2006). The dotted black line shows the percentage of land grid boxes with valid data in each year. (Source: GHCNDEX.)

The number of warm days is high over Europe and Australia from GHCNDEX (Plate 2.1c),

Table 2.2. WMO Expert Team on Climate Change Detection and Indices (ETCCDI; Zhang et al. 2011) temperature indices used in this section and their definitions.

Index	Name	Definition
TX90p	Warm days	Count of days where the maximum temperature was above the climatological 90th percentile (defined over 1961–90, days)
TN10p	Cool nights	Count of days where the minimum temperature was below the climatological 10th percentile (defined over 1961–90, days)
TNx	Maximum "night-time" temperature	Warmest minimum temperature (TN, °C)